

---

# Characterizing Detectability in 3DGS Poisoning: A Stage-wise Benchmark

---

Quoc-Anh Bui-Huynh<sup>1,2,3</sup> Thanh Duc Ngo<sup>2,3</sup> Xue Geng<sup>4</sup> Kaixin Xu<sup>4</sup>  
Wang Zhe<sup>4</sup> Xulei Yang<sup>4</sup> Ngai-Man Cheung<sup>1\*</sup>

<sup>1</sup>Temasek Laboratories, Singapore University of Technology and Design

<sup>2</sup>Vietnam National University, Ho Chi Minh City <sup>3</sup>University of Information Technology, VNU-HCM

<sup>4</sup>Agency for Science, Technology, and Research (A\*STAR)

{huynh\_bui, ngaiman\_cheung}@sutd.edu.sg thanhnd@uit.edu.vn  
{geng\_xue, xu\_kaixin, zhe\_wang, yang\_xulei}@a-star.edu.sg

## Abstract

3D Gaussian Splatting (3DGS) has rapidly emerged as a leading representation for real-time novel view synthesis, but recent work has shown that it is vulnerable to diverse poisoning attacks, including illusory object injection, computation cost amplification, and post hoc model watermarking. Despite this expanding threat surface, existing studies primarily focus on attack success, while defense and detection remain underexplored. From a detection perspective, a key challenge and opportunity arise from the multi-stage nature of the 3DGS reconstruction pipeline, which produces heterogeneous intermediate representations. Importantly, forensic signals for detecting poisoning are inherently stage dependent: an attack introduced at one stage may produce signals that emerge only at later stages or become more detectable as the pipeline progresses. This motivates a *stage-wise view of detectability* that goes beyond single-stage evaluation. **In this work**, we introduce **Poison-3DGS**, a benchmark designed for *stage-wise characterization of poisoning detection in 3DGS*. The benchmark exposes stage-specific artifacts, including multi-view images, geometry, training dynamics, and Gaussian parameters, and covers a diverse set of scenes and poisoning attacks. Using this benchmark, we conduct a systematic study of detectability across pipeline stages. Our analysis reveals several key insights. First, detectability varies significantly across stages, and no single stage consistently dominates across attack types. Second, different attacks exhibit distinct stage-specific forensic signals, indicating that detection effectiveness depends critically on where signals are observed. Third, later stage signals such as training dynamics and Gaussian parameter statistics provide strong cues that are not observable at earlier stages, where the attack is introduced or remains less detectable. Overall, our work provides a principled benchmark and the first systematic characterization of stage-dependent detectability in 3DGS, offering a foundation for future research on robust and reliable 3DGS systems. **We include the benchmark in the submission.**

## 1 Introduction

3D Gaussian Splatting (3DGS) [16, 3] has recently emerged as a leading representation for real-time photorealistic scene reconstruction, with growing deployment in robotics, augmented and virtual reality, mapping, and content creation [39, 5, 27]. As 3DGS moves into production pipelines, the integrity of its training inputs and intermediate artifacts becomes a concrete security concern.

---

\*Corresponding author.

A growing number of poisoning attacks now target 3DGS under fundamentally different threat models. StealthAttack [15] composites an illusory object into a target view and injects Gaussian seed points into low-density voids of the Structure-from-Motion (SfM) point cloud [28]. Poison-Splat [24] adds bounded adversarial noise to training images and forces the optimizer to over-densify, inflating Gaussian count, GPU memory, and training time by a factor of two to seven. Meanwhile, 3D-GSW [13] finetunes a trained model to embed a decodable covert watermark in Gaussian colour, opacity, rotation, and scale, while leaving positions and the training trajectory untouched. GuardSplat [7] similarly modifies a pre-trained model by embedding messages into spherical harmonic features while preserving geometry and rendering fidelity. Although originally proposed for watermarking or ownership protection, such post-training modifications alter the learned representation to encode hidden information. In this work, we adopt a broad definition of poisoning that includes any unauthorized intervention modifying the learned 3DGS representation. These attacks therefore span data-level, training-level, and model-level interventions across the 3DGS pipeline, from input data to final model representation.

**Research Gap.** Existing 3DGS attack studies [15, 7, 13, 24] focus on attacker-centric metrics, such as visual stealth, Gaussian inflation ratio, or watermark recovery accuracy, but lack a systematic, defender-centric evaluation of detectability. From a detection perspective, a key challenge and opportunity arise from the multi-stage nature of the 3DGS reconstruction pipeline. The process involves stage-specific artifacts, including multi-view images, geometry, training dynamics, and Gaussian parameters. As a result, forensic signals for detecting poisoning are inherently *stage dependent*. Importantly, an attack introduced at one stage may produce an attack footprint whose corresponding forensic signal emerges only at later stages or becomes more detectable as the pipeline progresses. This multi-stage structure creates both challenges and opportunities for detection, as different stages expose distinct and complementary evidence, a property that is particularly pronounced in 3DGS compared to conventional data poisoning settings.

This motivates a deeper view of 3DGS poisoning detection: beyond asking whether detection is possible, it is important to study *where* forensic signals arise and become detectable, and *how* different stages contribute to detectability. While detection has been extensively studied in 2D image forensics [8, 23, 29] and 3D anomaly detection [41], these settings typically assume a single representation or uniform access to data. In contrast, 3DGS is a multi-stage pipeline where detection performance depends on which stage is analyzed. Despite this, there is no unified framework or benchmark that enables systematic, stage wise characterization of forensic signals or reveals detection effectiveness across different stages of the 3DGS pipeline.

**In this paper**, we address this gap by introducing **Poison-3DGS**, a benchmark for studying 3DGS poisoning detection from a stage wise perspective. Building on the stage-dependent view illustrated in Fig. 1, we move beyond treating detection as a single-stage problem and instead characterize how forensic signals arise and become informative across the 3DGS pipeline. To this end, Poison-3DGS is designed to expose stage-specific artifacts and enable systematic analysis of detectability across different stages. Using this benchmark, we conduct a comprehensive study across representative attacks and derive key insights into stage-dependent detection behavior. Our contributions are summarized as follows.

- **Stage-wise characterization of forensic signals.** We identify that in 3DGS poisoning, forensic signals are inherently stage-dependent due to the multi-stage reconstruction pipeline. An attack introduced at one stage may produce signals that emerge only at later stages or become more detectable as the pipeline progresses. This perspective reframes detection as understanding where informative signals arise across the pipeline.
- **Benchmark grounded in stage-wise design.** We construct **Poison-3DGS**, a benchmark that exposes stage-specific artifacts including multi-view images, geometry, training dynamics, and Gaussian parameters. This design enables controlled and systematic characterization of how different stages contribute to detectability, providing a principled framework beyond conventional single-stage evaluation.
- **Empirical insights on stage-dependent detectability.** Using Poison-3DGS, we show that detectability varies significantly across stages, and no single stage consistently dominates across attack types. In particular, later stage signals such as training dynamics and Gaussian parameter statistics provide strong cues that are not observable at earlier stages, where the attack is introduced or remains less detectable. This reveals new opportunities for detection.

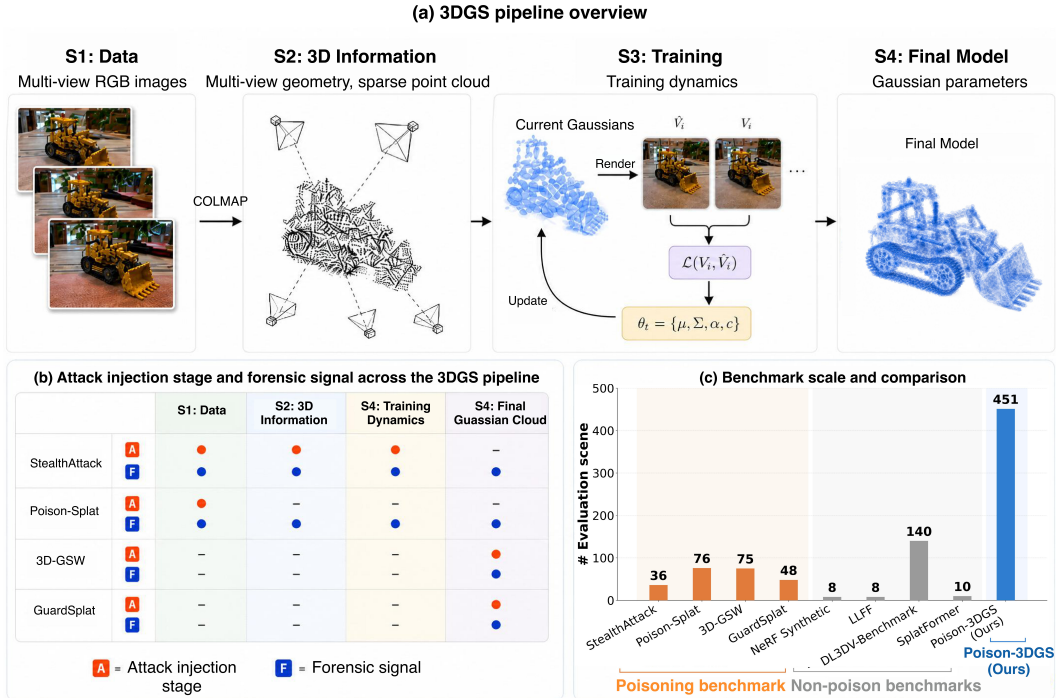


Figure 1: **Our stage-wise view of 3DGS poisoning detection.** (a) The multi-stage 3DGS reconstruction pipeline exposes *stage-specific artifacts*, including multi-view images, geometry, training dynamics, and Gaussian parameters. (b) *Attack injection stages* and their corresponding *forensic signals* across the pipeline. An attack introduced at one stage may produce its most detectable forensic signal at a different stage. (c) In addition to large scale and coverage, our benchmark supports stage-wise characterization of detectability and analysis of distinct and complementary forensic signals at different stages. The stage-wise formulation enables understanding of the contribution of individual sources of evidence.

- **Stage-specific signatures of different attacks.** We demonstrate that different attacks exhibit distinct stage-specific signatures. For example, StealthAttack is most detectable at data and training dynamic, Poison-Splat, 3D-GSW, and GuardSplat at the final model stage. These results highlight the importance of stage-aware analysis for understanding attack behavior.
- **Stage-aware detector design and adaptation.** We develop and adapt detectors to operate on stage-specific artifacts across the 3DGS pipeline, including multi-view images, geometry, training dynamics, and Gaussian parameters. Where suitable methods exist, we extend them to handle 3DGS-specific artifacts; where they do not, we design simple stage-specific detectors to capture relevant forensic signals. Our results show that off-the-shelf detectors transfer poorly across stages, while stage-aware designs that exploit stage-specific artifacts achieve more reliable detection.

## 2 Related Work

**3DGS poisoning threats.** Recent work shows that 3D Gaussian Splatting is vulnerable to attacks that directly affect users of reconstructed scenes. StealthAttack [15] targets scene integrity by injecting viewpoint-dependent illusory content through coordinated image and SfM manipulation, while Poison-Splat [24] targets availability by perturbing training images to trigger excessive densification, increasing Gaussian count, memory use, and training cost. Although watermarking methods such as 3D-GSW [13] and GuardSplat [7] are designed for ownership protection, they also demonstrate that a converged 3DGS model can be modified directly at the final Gaussian representation to encode hidden information while preserving visual quality. GaussTrap [10] further shows that poisoned views can induce targeted scene confusion. These studies establish a growing threat surface for 3DGS, but their evaluations remain mostly attack-centric: each work studies its own scenes, artifacts, and

success criteria. Poison-3DGS instead studies these manipulations under a unified detector-centric protocol, with the goal of characterizing where forensic signals become observable across the 3DGS pipeline.

**Defender-side evidence for 3DGS poisoning.** Defender-side analysis of poisoning attacks is commonly framed as an evidence-discovery problem [35, 20]: suspicious inputs may be detected through image forensic cues [14], poisoned samples may appear as representation outliers, and abnormal training behavior may reveal attack-specific learning dynamics [8, 23, 31, 11]. For 3DGS, this evidence-discovery problem is naturally structured by the reconstruction pipeline, which exposes multiple artifact types, including raw images, SfM geometry, optimization traces, and final Gaussian parameters. Recent 3DGS defenses have begun to exploit parts of this pipeline, especially for computation-cost attacks: RemedyGS detects and purifies poisoned input images, while Spectral Defense suppresses attack-induced Gaussian growth through frequency-based filtering and regularization [19, 4]. These methods provide important mitigation mechanisms for specific threat settings. Complementary to them, Poison-3DGS focuses on systematic evaluation; it provides a unified defender-centric protocol for characterizing where forensic signals become observable across different attack families and stage-specific 3DGS artifacts.

### 3 Preliminaries: 3D Gaussian Splatting

3D Gaussian Splatting (3DGS) [16] represents a scene as a set of anisotropic Gaussian primitives  $\mathcal{G} = \{g_i\}_{i=1}^N$ . Each Gaussian  $g_i = (\mu_i, \Sigma_i, \alpha_i, c_i)$  contains a 3D center  $\mu_i$ , covariance  $\Sigma_i$ , opacity  $\alpha_i$ , and view-dependent color coefficients  $c_i$ . Given posed multi-view images  $\mathcal{D} = \{(V_k, \Pi_k)\}_{k=1}^K$ , where  $V_k$  is the ground-truth image and  $\Pi_k$  denotes the camera parameters, 3DGS renders a predicted view  $\hat{V}_k = \mathcal{R}(\mathcal{G}; \Pi_k)$  through differentiable splatting and alpha compositing.

Training optimizes the Gaussian parameters by minimizing a photometric reconstruction loss:

$$\min_{\mathcal{G}} \mathcal{L}_{\text{photo}}(\mathcal{D}) = \min_{\mathcal{G}} \sum_{k=1}^K \left[ (1 - \lambda) \mathcal{L}_1(\hat{V}_k, V_k) + \lambda \mathcal{L}_{\text{D-SSIM}}(\hat{V}_k, V_k) \right], \quad \hat{V}_k = \mathcal{R}(\mathcal{G}; \Pi_k), \quad (1)$$

where  $\lambda$  balances pixel-wise and structural reconstruction terms. During optimization, 3DGS also performs adaptive density control, which dynamically adds and removes Gaussian primitives. Gaussians with large view-space positional gradients are densified through cloning or splitting, while Gaussians with low opacity are pruned. This process allows 3DGS to allocate more capacity to regions that remain difficult to reconstruct, but it also makes the number of Gaussians and their parameter statistics part of the training dynamics.

## 4 Poison-3DGS: Benchmarking Stage-wise Poisoning Detectability

### 4.1 A Defender-centric Benchmark Setup

Existing 3DGS security works are primarily attack-centric: they evaluate whether an injected object appears, whether perturbations remain imperceptible, whether computation cost increases, or whether a watermark can be decoded. These metrics validate attack success, but they do not answer the defender-side question studied here: at which stage of the 3DGS pipeline can poisoning be detected? Prior poisoning and watermarking papers evaluate their own threat models in isolation, often with different scenes, artifacts, and success. Poison-3DGS instead turns heterogeneous 3DGS attacks into a unified stage-wise detection benchmark.

**Stage-wise characterization of poisoning detection.** Poison-3DGS studies poisoning detection under a unified detector-centric protocol over four stage-specific artifact groups: **S1: Data**, raw multi-view RGB images; **S2: 3D Information**, SfM cameras, tracks, and sparse points; **S3: Training Dynamics**, render-loss-update behavior including losses, gradients, densification, and Gaussian growth; and **S4: Final Model**, trained Gaussian parameters and rendered outputs. Each detector operates on the artifact group of a given stage and produces a scene-level anomaly score.

This stage-wise view is necessary because the *attack injection stage* and the *forensic signal* are often decoupled. The attack injection stage is the artifact directly manipulated by the adversary, while the forensic signal is the evidence that remains observable after the pipeline processes that

manipulation. For example, Poison-Splat perturbs images at **S1**, but its clearest signal appears later through abnormal densification at **S3** and abnormal final Gaussian statistics at **S4**. Conversely, post-training model-level attacks may leave no evidence in the input data, SfM reconstruction, or training dynamics, but become observable only in the final Gaussian model. Thus, Poison-3DGS evaluates not only whether a scene is poisoned, but also *where* its forensic signal becomes observable.

**Dataset.** Poison-3DGS contains 37 clean scenes drawn from Free [34], Mip-NeRF 360 [2], and Tanks-and-Temples [17]. The scenes cover handheld captures, indoor and outdoor environments, object-centric reconstructions, unbounded scenes, and large architectural captures. For each scene, we provide raw images, SfM reconstruction, training checkpoints, and a matched clean 3DGS reference model. Each poisoned variant is paired with its clean counterpart, which makes scene-level binary detection well-defined and allows detectors to be compared under the same scene distribution.

**Attack Space.** Poison-3DGS, illustrated in Fig. 2, includes four attack families spanning data-level, geometry-level, training-time, and final-model interventions. Rather than reproducing each attack in a single isolated setting, we expand them into controlled variants that expose factors relevant to detectability. For StealthAttack [15], we scale the illusory-object setting to 30 object identities and vary object size and target-view difficulty, yielding 120 variants. For Poison-Splat [24], we vary the perturbation budget and poisoned-view ratio, including practical partial-poisoning settings. For 3D-GSW [13] and GuardSplat [7], we vary message length and embedding strength while preserving their distinct final-model interventions: 3D-GSW modifies broader Gaussian attributes, whereas GuardSplat concentrates its changes in spherical-harmonic coefficients. Overall, Poison-3DGS contains 414 poisoned variants, enabling controlled analysis of how attack surfaces and attack parameters shape stage-specific forensic signals. See Appendix ?? for more examples.

**Metrics and Protocol.** We formulate poisoning detection as binary scene-level detection, with clean scenes as negatives and poisoned variants as positives. Each detector assigns a real-valued anomaly score to a scene at a given stage, and scenes are ranked by this score for evaluation. Following score-based detector evaluation protocols in OOD and anomaly detection [9, 18, 37], we report AUROC to measure overall separability between clean and poisoned scenes, and FPR@95TPR to measure the false-alarm rate when detecting 95% of poisoned variants. When a detector produces image-level, view-level, point-level, checkpoint-level, or Gaussian-level scores, we aggregate them into a single scene-level score using the detector-specific aggregation rule. Clean and poisoned variants of the same scene use matched evaluation views, so detector scores and reconstruction metrics are computed on comparable observations. For StealthAttack and Poison-Splat, we use a fixed 3DGS training schedule and record per-iteration diagnostics; for 3D-GSW and GuardSplat, we provide the modified final Gaussian models, embedding logs, and rendered outputs. We report both per-attack results and pooled results across attack families.

## 4.2 A Detector Suite for Stage-specific Forensic Signals

To evaluate poisoning detectability across the 3DGS pipeline, we construct an unsupervised detector suite matched to the artifact group exposed at each stage. For fairness, all detectors use official pretrained weights or released off-the-shelf checkpoints, with no poisoned-sample fine-tuning, attack-specific adaptation, or access to attack labels. Each detector receives only its corresponding stage artifact and produces scene-level anomaly scores via stage-appropriate aggregation.

**S1: Data.** At the data stage, detectors operate on the raw multi-view training images  $\mathcal{V} = \{V_k\}_{k=1}^K$ . A data-stage attack modifies a subset of views  $\mathcal{P}$  and produces manipulated images  $V'_k = \mathcal{A}(V_k)$  for  $k \in \mathcal{P}$ , such as the target-view insertion in StealthAttack or the adversarial perturbations in Poison-Splat. We evaluate MVSS-Net [8], IML-ViT [26], and SparseViT [29] by applying each detector  $f_\psi$  independently to every training view, yielding a view-level score  $s_k = f_\psi(V_k)$ , or  $s'_k = f_\psi(V'_k)$  for a manipulated view. Since poisoning can affect a small subset of views, we aggregate view-level scores by max pooling,  $S_{\text{scene}} = \max_k s_k$ . We also include SoftPatch+ [32], which estimates patch-level outlier scores and calibrates them using images from the same scene before producing a scene-level score. These baselines test whether poisoning is already visible as image-level forensic signals before SfM reconstruction or 3DGS optimization.

**S2: 3D Information.** At the 3D information stage, we ask whether manipulated views become observable after SfM reconstruction. Given the input views, COLMAP recovers camera intrinsics/extrinsics, feature tracks, and a sparse point cloud  $\mathcal{X} = \{x_j\}_{j=1}^N$  formed by triangulated 3D

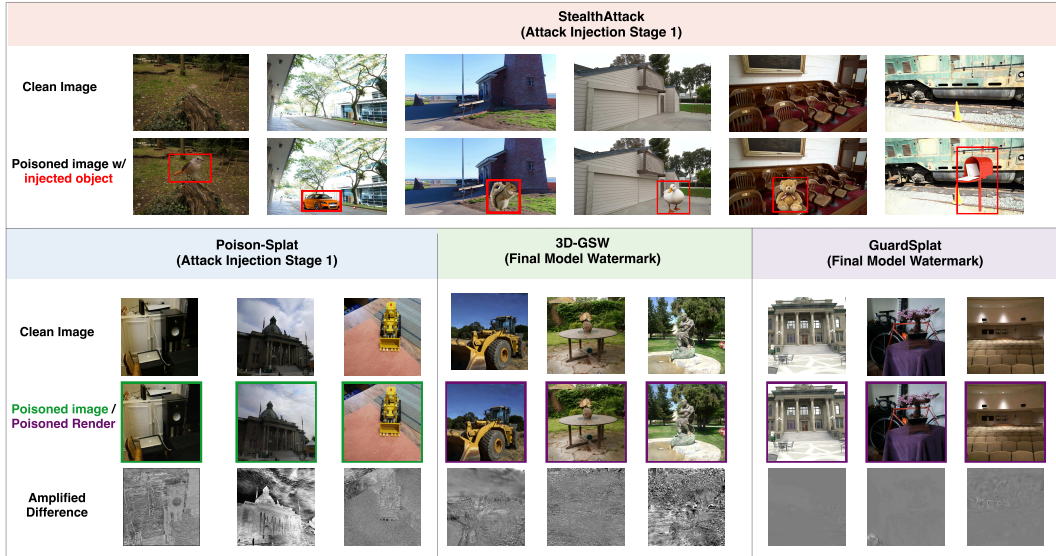


Figure 2: Qualitative examples from **Poison-3DGS**. **StealthAttack** shows *image injection* by inserting an illusory object into a target training image, while **Poison-Splat** shows *image perturbation* through subtle adversarial noise and its amplified residual. For **3D-GSW** and **GuardSplat**, we render the same sample view from the clean model and the watermarked model, and visualize amplified differences. The figure illustrates that different attack families in our benchmark leave distinct forensic signal at different stages of the 3DGS pipeline.

points. This stage exposes two complementary forensic signals. First, manipulated views may violate multi-view consistency: an inserted object may be supported only by the target view, while adversarial perturbations may disturb feature matching, correspondence, or view-consistent geometry. We therefore use MET3R [1], MV-DUST3R+ [30], NoPoSplat [38], and VGGT [33] as multi-view consistency probes. Their reconstruction or consistency error is used as a geometric anomaly score  $s_{\text{geo}}$  and aggregated into a scene-level score using the same max-pooling strategy as S1. Second, injection-based attacks can leave sparse-geometry anomalies; for example, **StealthAttack** may introduce artificial points along the object ray, creating abnormal local density or geometry in  $\mathcal{X}$ . To capture this signal, we extract per-point features from coordinates, RGB colors, and estimated normals using Sonata [36] or Concerto [40], then fit an Isolation Forest [22] within each scene to score local geometric irregularities.

**S3: Training Dynamics.** At the training stage, detectors operate on optimization diagnostics from saved 3DGS states  $\theta_t = \{g_i^t\}_{i=1}^{M_t}$ , where the number of Gaussians  $M_t$  changes over training due to densification and pruning. Unlike fixed-network gradient monitoring, this setting has a dynamic parameter set, no shared layer-wise embedding space across scenes, and view-dependent supervision: each training view affects only the Gaussians visible in its camera frustum. Nevertheless, poisoning can leave distinctive optimization fingerprints. For example, **StealthAttack** biases early optimization toward reconstructing the target-view illusion, while **Poison-Splat** is a DoS-style attack that induces excessive Gaussian growth and GPU memory cost. We therefore construct gradient-based baselines adapted to 3DGS dynamics. At each saved optimization state  $\theta_t$ , we summarize per-Gaussian update magnitudes, such as the positional-gradient norm  $|\nabla_{x_i} \mathcal{L}(\theta_t)|_2$ . We then aggregate these magnitudes across the visible Gaussians within each training view, yielding a view-indexed gradient matrix that captures how strongly each view drives the optimization. From this matrix, we derive scene-level anomaly scores using two unsupervised baselines: a GradNorm-style score over heavy-tailed gradient magnitudes [12], and a Spectral-style score over the leading singular component of this matrix [31]. These baselines test whether poisoning can be detected from optimization behavior before inspecting the final Gaussian representation.

**S4: Final Model.** At the final-model stage, detectors operate on the optimized Gaussian representation  $\mathcal{G}^* = \{g_i\}_{i=1}^M$ , where each Gaussian stores geometry and appearance attributes. This stage is security-critical because  $\mathcal{G}^*$  is the artifact ultimately rendered, shared, or deployed, and it may carry forensic

Table 1: Stage-wise detector performance across poisoning attacks. Rows are grouped by the 3DGS pipeline stage at which each detector operates. Entries report scene-level AUROC and FPR@95. Overall pools the attacks evaluated at that stage. “N/A” indicates that the attack does not expose forensic signals at that stage or that the required artifact is structurally unavailable. Bold denotes the best result for each attack-specific column among applicable methods.

Methods	Overall		StealthAttack		Poison-Splat		3D-GSW		GuardSplat	
	AUROC↑	FPR@95↓	AUROC↑	FPR@95↓	AUROC↑	FPR@95↓	AUROC↑	FPR@95↓	AUROC↑	FPR@95↓
<i>S1: Data multi-view images</i>										
IML-ViT (arXiv’24) [26]	0.591	0.892	0.666	0.892	0.496	0.892	N/A	N/A	N/A	N/A
MVSS-Net (TPAMI’22) [8]	0.414	0.973	0.511	0.919	0.290	1.000	N/A	N/A	N/A	N/A
SparseViT (AAAI’25) [29]	0.550	0.946	0.636	0.892	0.440	1.000	N/A	N/A	N/A	N/A
SoftPatch+ (PR’25) [32]	0.617	0.973	0.768	<b>0.622</b>	0.423	1.000	N/A	N/A	N/A	N/A
<i>S2: 3D Information multi-view geometry</i>										
MET3R (CVPR’25) [1]	0.585	0.838	0.578	0.811	0.594	0.892	N/A	N/A	N/A	N/A
MV-DUSi3R+ (CVPR’25) [30]	0.525	0.973	0.481	0.973	0.581	0.973	N/A	N/A	N/A	N/A
NoPoSplat (ICLR’25) [38]	0.429	0.973	0.480	1.000	0.365	0.946	N/A	N/A	N/A	N/A
VGGT (CVPR’25) [33]	0.487	1.000	0.520	0.973	0.445	1.000	N/A	N/A	N/A	N/A
<i>S2: 3D Information sparse point cloud</i>										
Sonata (CVPR’25) [36]	0.766	0.892	0.766	0.892	N/A <sup>†</sup>	N/A <sup>†</sup>	N/A	N/A	N/A	N/A
Concerto (NeurIPS’25) [40]	0.725	0.946	0.725	0.946	N/A <sup>†</sup>	N/A <sup>†</sup>	N/A	N/A	N/A	N/A
<i>S3: Training training dynamics</i>										
GradNorm-style <sup>†</sup> (NeurIPS’21) [12]	0.687	0.919	<b>0.780</b>	0.784	0.538	0.919	N/A	N/A	N/A	N/A
Spectral-style <sup>†</sup> (NeurIPS’18) [31]	0.582	0.919	0.572	0.919	0.598	0.919	N/A	N/A	N/A	N/A
<i>S4: Final Model Gaussian parameters</i>										
SceneSplat (ICCV’25) [21]	0.528	0.973	0.591	0.865	0.492	0.973	0.568	0.973	0.426	0.973
SplatFormer (ICLR’25) [6]	0.619	0.946	0.681	0.946	0.594	0.784	<b>0.689</b>	<b>0.919</b>	0.478	0.973
Gaussian-MAE (3DV’25) [25]	0.601	0.919	0.568	0.919	<b>0.806</b>	<b>0.486</b>	0.570	0.919	<b>0.488</b>	<b>0.973</b>

<sup>†</sup> These training-stage baselines are adapted to 3DGS training dynamics rather than used as direct classifier-level detectors. We report S3 results at the fixed checkpoint training iteration for all attacks and the overall split. <sup>‡</sup> Sparse point-cloud detectors are evaluated only when the poisoned artifact affects or exposes the SfM point cloud. For Poison-Splat, the original setup uses sparse point clouds generated from clean images, so this artifact is structurally unavailable for detecting the attack.

signals from input- or training-stage attacks (e.g., StealthAttack’s illusory object or Poison-Splat’s over-densified Gaussian cloud) as well as post-training modifications from 3D-GSW or GuardSplat. We use SceneSplat [21], SplatFormer [6], and Gaussian-MAE [25] as frozen Gaussian encoders, providing complementary feature spaces through scene-level representation learning, Gaussian refinement, and masked Gaussian-attribute reconstruction. For each scene, the final Gaussian cloud  $\mathcal{G}_i^*$  is independently encoded into a normalized scene embedding  $\hat{z}_i$ . We summarize the clean reference set by its normalized centroid  $\hat{\mu}$ , and score each scene by its deviation from this clean prototype using negative cosine similarity,  $s_i = -\hat{z}_i^\top \hat{\mu}_{(i)}$ , with a leave-one-out centroid when scoring a clean reference scene. This produces a scene-level anomaly score in the learned Gaussian feature space, where larger values indicate greater deviation from the clean final-model distribution.

## 5 Analysis: Stage-specific Detectability and Detector Alignment

We analyze Poison-3DGS from a defender-centric perspective: where poisoning becomes detectable in the 3DGS pipeline, and which detectors capture the corresponding forensic signals. Rather than treating detection as a single decision over a completed scene, we study how forensic signals appear across stage-specific artifacts, how they differ across attack families, and how detector performance depends on the artifact being analyzed. Each detector follows our stage-specific access protocol: it only uses artifacts available at its corresponding 3DGS stage and outputs a scene-level anomaly score.

### 5.1 Stage-specific Detectability Across Attacks

**Where do forensic signals become most detectable?** Table 1 shows that detectability varies substantially across stages, and no single stage consistently dominates across attack families. This supports a stage-wise view of 3DGS poisoning detection: the most informative forensic signal depends on how each attack interacts with the reconstruction pipeline.

StealthAttack leaves forensic signals across multiple stages. Its target-view insertion creates localized image evidence at S1, where the best image-stage detector reaches 0.768 AUROC. The injected geometry can also affect sparse 3D structure at S2. However, the strongest separation in our study appears at S3, where training dynamics reach 0.780 AUROC. This is consistent with the attack mechanism: the attack-specific noise scheduler perturbs clean-view supervision during training,

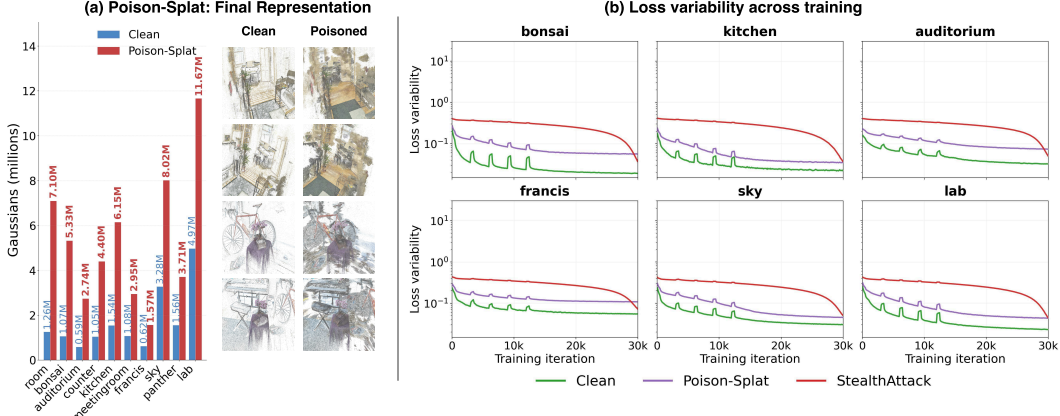


Figure 3: **Stage-specific forensic signals for different attacks.** (a) Poison-Splat is most visible in the *final Gaussian representation*: poisoned models contain more Gaussians and show denser Gaussian-center distributions than matched clean models, revealing *over-densification* rather than render-quality differences. (b) StealthAttack is most visible in *training dynamics*: its loss variability remains higher throughout optimization, indicating unstable view-wise supervision. These examples show that different attacks become most separable from different 3DGS artifacts.

making optimization less stable across views. As a result, the training trajectory exhibits elevated per-view loss variability and abnormal Gaussian update behavior.

Poison-Splat exhibits a different detectability profile. Although it is injected at S1 through bounded image perturbations, these perturbations are weakly visible at the image stage. Their effect is amplified later through 3DGS optimization. By interfering with adaptive density control, Poison-Splat induces excessive Gaussian growth, making the final Gaussian representation the most informative stage for detection. At S4, Gaussian-MAE reaches 0.806 AUROC, substantially higher than the image-stage result. As shown in Fig. 3, this appears as increased Gaussian count and denser Gaussian-center distributions.

Post-training attacks form a third case. Since 3D-GSW and GuardSplat modify the trained Gaussian representation after clean reconstruction, their forensic signals are only observable at S4 under our stage-specific access protocol. The current S4 detectors provide uneven separation: 3D-GSW reaches 0.689 AUROC with SplatFormer, while GuardSplat remains difficult, with the best AUROC only 0.488. This suggests that final-model access is necessary for these attacks, but not sufficient unless the detector is aligned with the specific Gaussian attributes being modified.

**Finding 1:** Detectability varies significantly across stages, and no single stage consistently dominates across attack families.

## 5.2 Forensic Signals Can Emerge After Attack Injection

**Does the attack injection stage determine the detection stage?** In a multi-stage 3DGS pipeline, the artifact directly modified by the adversary is not always the artifact that provides the strongest forensic signal. Downstream processing can transform an early manipulation into later-stage evidence through SfM reconstruction, optimization, or final Gaussian parameterization. Therefore, evaluating only the attack injection stage may miss where poisoning becomes most observable.

Poison-Splat and StealthAttack illustrate this decoupling. Poison-Splat is injected at S1 through image perturbations, but its image-stage separability remains weak, with the best S1 AUROC reaching only 0.496; its effect instead accumulates through optimization and becomes clearer as Gaussian over-densification at S4. StealthAttack is introduced through target-view image and geometry manipulation, making S1 and S2 informative, but its attack-specific training schedule further disrupts view-wise optimization, making S3 the most separable stage in our detector suite. These cases show that 3DGS poisoning should be analyzed as a pipeline process, not only at the point of attack injection.

*Finding 2:* Attack injection and strongest detectability are not always aligned.

### 5.3 Detector Alignment with Stage-specific Forensic Signals

**Which detectors capture the relevant forensic signals, and why?** Table 1 shows that existing detectors transfer unevenly across stage-specific 3DGS artifacts. This unevenness reflects whether each detector is aligned with the forensic signal exposed at its stage. For StealthAttack, SoftPatch+ is effective at S1 because the attack edits only a few views and the inserted object is spatially localized; patch-level, scene-calibrated scoring preserves this local evidence better than a global image score. At S3, the GradNorm-style detector performs best because StealthAttack’s noise scheduler perturbs clean-view supervision during training, producing unstable view-wise optimization and abnormal per-Gaussian update magnitudes.

For Poison-Splat, Gaussian-MAE performs best among S4 detectors because its pretext task is closest to the attack’s final-model forensic signal. Poison-Splat mainly changes the distribution of Gaussian primitives after abnormal densification, including count, density, scale, opacity, and geometry, rather than semantic scene content. Gaussian-MAE learns from Gaussian splats through masked reconstruction of primitive attributes, making it more sensitive to such local parameter changes. In contrast, SceneSplat is designed for 3DGS scene understanding with vision-language pretraining, while SplatFormer targets feed-forward refinement of Gaussian splats for robust novel-view rendering; these objectives are less directly aligned with detecting abnormal primitive distributions. Consistently, Table 1 shows that Gaussian-MAE reaches 0.806 AUROC on Poison-Splat, compared with 0.492 for SceneSplat and 0.594 for SplatFormer. SceneSplat’s focus on 3DGS scene understanding with vision-language pretraining and SplatFormer’s focus on refinement for robust novel-view synthesis support this interpretation.

The same alignment principle explains the different outcomes for 3D-GSW and GuardSplat. Both are post-training attacks observable only at S4 under our protocol, but they modify different Gaussian attributes. 3D-GSW applies a broader intervention over Gaussian geometry and appearance, producing a more detectable final-representation shift, with SplatFormer reaching 0.689 AUROC. GuardSplat is narrower: its signal is concentrated in spherical-harmonic appearance coefficients while preserving geometry and rendering quality, so current S4 detectors remain weak, with the best AUROC only 0.488. Thus, final-model access is necessary but not sufficient; detectors must also match the specific Gaussian attributes modified by the attack.

*Finding 3:* Existing detectors transfer unevenly across stage-specific 3DGS artifacts.

## 6 Conclusion and Discussion

This paper studies poisoning detection in 3D Gaussian Splatting from a stage-wise, defender-centric perspective. While recent attacks manipulate input views, SfM geometry, training dynamics, and final Gaussian parameters, existing evaluations mainly focus on attack success rather than where evidence becomes detectable. We introduce **Poison-3DGS**, a benchmark for characterizing poisoning detection across 3DGS pipeline stages, exposing artifacts from multi-view images, geometry, training traces, and Gaussian parameters. Our study shows that detectability varies substantially across stages, no single stage consistently dominates across attack types, and attack injection and strongest detectability are often decoupled. We further find that detector effectiveness depends on alignment with stage-specific forensic signals, suggesting that 3DGS security should be treated as a pipeline-level problem rather than a single-artifact detection task. We hope Poison-3DGS provides a foundation for future work on robust and reliable 3DGS systems.

**Limitations and future directions.** Poison-3DGS is built on the current public landscape of 3DGS attacks, using official or reproducible implementations whenever available. As new attacks emerge, the benchmark can be extended while preserving its core design: matched clean references, stage-wise artifacts, and scene-level detector evaluation.

1. **Extending the attack suite.** Future extensions can incorporate new poisoning, watermarking, or model-manipulation attacks by applying them to the same clean scene pool, recording their

pipeline artifacts, and evaluating them under the same unified detector protocol. This would allow new threats to be compared by both attack success and where their forensic signals emerge across the 3DGS pipeline.

2. **From detection to mitigation.** Poison-3DGS characterizes where forensic signals become observable, but does not propose a complete mitigation method. This motivates stage-aware defenses, such as filtering suspicious views, repairing SfM geometry, regularizing abnormal densification, or auditing final Gaussian attributes before deployment.

## References

- [1] Mohammad Asim, Christopher Wewer, Thomas Wimmer, Bernt Schiele, and Jan Eric Lenssen. Met3r: Measuring multi-view consistency in generated images. In *Proceedings of the IEEE/CVF Conference on Computer Vision and Pattern Recognition (CVPR)*, pages 6034–6044, June 2025.
- [2] Jonathan T Barron, Ben Mildenhall, Dor Verbin, Pratul P Srinivasan, and Peter Hedman. Mipnerf 360: Unbounded anti-aliased neural radiance fields. In *Proceedings of the IEEE/CVF conference on computer vision and pattern recognition*, pages 5470–5479, 2022.
- [3] Guikun Chen and Wenguan Wang. A survey on 3d gaussian splatting. *ACM Computing Surveys*, 2024.
- [4] Yang Chen, Yi Yu, Jiaming He, Yueqi Duan, Zheng Zhu, and Yap-Peng Tan. Spectral defense against resource-targeting attack in 3d gaussian splatting. *arXiv preprint arXiv:2603.12796*, 2026.
- [5] Yiwen Chen, Zilong Chen, Chi Zhang, Feng Wang, Xiaofeng Yang, Yikai Wang, Zhongang Cai, Lei Yang, Huaping Liu, and Guosheng Lin. Gaussianeditor: Swift and controllable 3d editing with gaussian splatting. In *Proceedings of the IEEE/CVF conference on computer vision and pattern recognition*, pages 21476–21485, 2024.
- [6] Yutong Chen, Marko Mihajlovic, Xiyi Chen, Yiming Wang, Sergey Prokudin, and Siyu Tang. Splatformer: Point transformer for robust 3d gaussian splatting, 2025.
- [7] Zixuan Chen, Guangcong Wang, Jiahao Zhu, Jianhuang Lai, and Xiaohua Xie. Guardsplat: efficient and robust watermarking for 3d gaussian splatting. In *Proceedings of the Computer Vision and Pattern Recognition Conference*, pages 16325–16335, 2025.
- [8] Chengbo Dong, Xinru Chen, Ruohan Hu, Juan Cao, and Xirong Li. Mvss-net: Multi-view multi-scale supervised networks for image manipulation detection. *IEEE Transactions on Pattern Analysis and Machine Intelligence*, 45(3):3539–3553, 2022.
- [9] Dan Hendrycks and Kevin Gimpel. A baseline for detecting misclassified and out-of-distribution examples in neural networks. *arXiv preprint arXiv:1610.02136*, 2016.
- [10] Jiaxin Hong, Sixu Chen, Shuoyang Sun, Hongyao Yu, Hao Fang, Yuqi Tan, Bin Chen, Shuhan Qi, and Jiawei Li. Gausstrap: Stealthy poisoning attacks on 3d gaussian splatting for targeted scene confusion, 2025. URL <https://arxiv.org/abs/2504.20829>.
- [11] Haoqi Huang, Ping Wang, Jianhua Pei, Jiacheng Wang, Shahen Alexanian, and Dusit Niyato. Deep learning advancements in anomaly detection: A comprehensive survey. *IEEE Internet of Things Journal*, 2025.
- [12] Rui Huang, Andrew Geng, and Yixuan Li. On the importance of gradients for detecting distributional shifts in the wild. In *Proceedings of the 35th International Conference on Neural Information Processing Systems, NIPS '21*, Red Hook, NY, USA, 2021. Curran Associates Inc. ISBN 9781713845393.
- [13] Youngdong Jang, Hyunje Park, Feng Yang, Heeju Ko, Euijin Choo, and Sangpil Kim. 3d-gsw: 3d gaussian splatting for robust watermarking. In *Proceedings of the Computer Vision and Pattern Recognition Conference*, pages 5938–5948, 2025.

- [14] VijayaKumar Kadha, Sambit Bakshi, and Santos Kumar Das. Unravelling digital forgeries: A systematic survey on image manipulation detection and localization. *ACM Computing Surveys*, 57(12):1–36, 2025.
- [15] Bo-Hsu Ke, You-Zhe Xie, Yu-Lun Liu, and Wei-Chen Chiu. Stealthattack: Robust 3d gaussian splatting poisoning via density-guided illusions. In *Proceedings of the IEEE/CVF International Conference on Computer Vision*, pages 27400–27411, 2025.
- [16] Bernhard Kerbl, Georgios Kopanas, Thomas Leimkühler, George Drettakis, et al. 3d gaussian splatting for real-time radiance field rendering. *ACM Trans. Graph.*, 42(4):139–1, 2023.
- [17] Arno Knapitsch, Jaesik Park, Qian-Yi Zhou, and Vladlen Koltun. Tanks and temples: Benchmarking large-scale scene reconstruction. *ACM Transactions on Graphics (ToG)*, 36(4):1–13, 2017.
- [18] Kimin Lee, Kibok Lee, Honglak Lee, and Jinwoo Shin. A simple unified framework for detecting out-of-distribution samples and adversarial attacks. *Advances in neural information processing systems*, 31, 2018.
- [19] Yanping Li, Zhening Liu, Zijian Li, Zehong Lin, and Jun Zhang. Remedygts: Defend 3d gaussian splatting against computation cost attacks. *arXiv preprint arXiv:2511.22147*, 2025.
- [20] Yiming Li, Yong Jiang, Zhifeng Li, and Shu-Tao Xia. Backdoor learning: A survey, 2022. URL <https://arxiv.org/abs/2007.08745>.
- [21] Yue Li, Qi Ma, Runyi Yang, Huapeng Li, Mengjiao Ma, Bin Ren, Nikola Popovic, Nicu Sebe, Ender Konukoglu, Theo Gevers, Luc Van Gool, Martin R. Oswald, and Danda Pani Paudel. Scenesplat: Gaussian splatting-based scene understanding with vision-language pretraining. In *Proceedings of the IEEE/CVF International Conference on Computer Vision (ICCV)*, pages 4961–4972, October 2025.
- [22] Fei Tony Liu, Kai Ming Ting, and Zhi-Hua Zhou. Isolation forest. In *2008 eighth IEEE international conference on data mining*, pages 413–422. IEEE, 2008.
- [23] Xuntao Liu, Yuzhou Yang, Haoyue Wang, Qichao Ying, Zhenxing Qian, Xinpeng Zhang, and Sheng Li. Multi-view feature extraction via tunable prompts is enough for image manipulation localization. In *Proceedings of the 32nd ACM International Conference on Multimedia*, pages 9999–10007, 2024.
- [24] Jiahao Lu, Yifan Zhang, Qihong Shen, Xinchao Wang, and Shuicheng Yan. Poison-splat: Computation cost attack on 3d gaussian splatting. *arXiv preprint arXiv:2410.08190*, 2024.
- [25] Qi Ma, Yue Li, Bin Ren, Nicu Sebe, Ender Konukoglu, Theo Gevers, Luc Van Gool, and Danda Pani Paudel. A large-scale dataset of gaussian splats and their self-supervised pretraining. In *2025 International Conference on 3D Vision (3DV)*, pages 145–155. IEEE, 2025.
- [26] Xiaochen Ma, Bo Du, Zhuohang Jiang, Xia Du, Ahmed Y. Al Hammadi, and Jizhe Zhou. Iml-vit: Benchmarking image manipulation localization by vision transformer, 2024. URL <https://arxiv.org/abs/2307.14863>.
- [27] Hidenobu Matsuki, Riku Murai, Paul HJ Kelly, and Andrew J Davison. Gaussian splatting slam. In *Proceedings of the IEEE/CVF conference on computer vision and pattern recognition*, pages 18039–18048, 2024.
- [28] Johannes Lutz Schönberger and Jan-Michael Frahm. Structure-from-motion revisited. In *Conference on Computer Vision and Pattern Recognition (CVPR)*, 2016.
- [29] Lei Su, Xiaochen Ma, Xuekang Zhu, Chaoqun Niu, Zeyu Lei, and Ji-Zhe Zhou. Can we get rid of handcrafted feature extractors? sparsevit: Nonsemantics-centered, parameter-efficient image manipulation localization through sparse-coding transformer. In *Proceedings of the AAAI conference on artificial intelligence*, volume 39, pages 7024–7032, 2025.

- [30] Zhenggang Tang, Yuchen Fan, Dilin Wang, Hongyu Xu, Rakesh Ranjan, Alexander Schwing, and Zhicheng Yan. Mv-dust3r+: Single-stage scene reconstruction from sparse views in 2 seconds. In *Proceedings of the IEEE/CVF Conference on Computer Vision and Pattern Recognition (CVPR)*, pages 5283–5293, June 2025.
- [31] Brandon Tran, Jerry Li, and Aleksander Madry. Spectral signatures in backdoor attacks. *Advances in neural information processing systems*, 31, 2018.
- [32] Chengjie Wang, Xi Jiang, Bin-Bin Gao, Zhenye Gan, Yong Liu, Feng Zheng, and Lizhuang Ma. Softpatch+: Fully unsupervised anomaly classification and segmentation. *Pattern Recognition*, 161:111295, 2025. ISSN 0031-3203. doi: <https://doi.org/10.1016/j.patcog.2024.111295>. URL <https://www.sciencedirect.com/science/article/pii/S003132032401046X>.
- [33] Jianyuan Wang, Minghao Chen, Nikita Karaev, Andrea Vedaldi, Christian Rupprecht, and David Novotny. Vggt: Visual geometry grounded transformer. In *Proceedings of the IEEE/CVF Conference on Computer Vision and Pattern Recognition (CVPR)*, pages 5294–5306, June 2025.
- [34] Peng Wang, Yuan Liu, Zhaoxi Chen, Lingjie Liu, Ziwei Liu, Taku Komura, Christian Theobalt, and Wenping Wang. F2-nerf: Fast neural radiance field training with free camera trajectories. In *Proceedings of the IEEE/CVF Conference on Computer Vision and Pattern Recognition*, pages 4150–4159, 2023.
- [35] Zhibo Wang, Jingjing Ma, Xue Wang, Jiahui Hu, Zhan Qin, and Kui Ren. Threats to training: A survey of poisoning attacks and defenses on machine learning systems. *ACM Comput. Surv.*, 55(7), December 2022. ISSN 0360-0300. doi: 10.1145/3538707. URL <https://doi.org/10.1145/3538707>.
- [36] Xiaoyang Wu, Daniel DeTone, Duncan Frost, Tianwei Shen, Chris Xie, Nan Yang, Jakob Engel, Richard Newcombe, Hengshuang Zhao, and Julian Straub. Sonata: Self-supervised learning of reliable point representations. In *Proceedings of the IEEE/CVF Conference on Computer Vision and Pattern Recognition (CVPR)*, pages 22193–22204, June 2025.
- [37] Jinkang Yang, Pengyun Wang, Dejian Zou, Zitang Zhou, Kunyuan Ding, Wenxuan Peng, Haoqi Wang, Guangyao Chen, Bo Li, Yiyu Sun, et al. Openood: Benchmarking generalized out-of-distribution detection. *Advances in Neural Information Processing Systems*, 35:32598–32611, 2022.
- [38] Botao Ye, Sifei Liu, Haofei Xu, Xueting Li, Marc Pollefeys, Ming-Hsuan Yang, and Songyou Peng. No pose, no problem: Surprisingly simple 3d gaussian splats from sparse unposed images, 2024. URL <https://arxiv.org/abs/2410.24207>.
- [39] Hongjia Zhai, Xiyu Zhang, Boming Zhao, Hai Li, Yijia He, Zhaopeng Cui, Hujun Bao, and Guofeng Zhang. Splatloc: 3d gaussian splatting-based visual localization for augmented reality. *IEEE Transactions on Visualization and Computer Graphics*, 2025.
- [40] Yujia Zhang, Xiaoyang Wu, Yixing Lao, Chengyao Wang, Zhuotao Tian, Naiyan Wang, and Hengshuang Zhao. Concerto: Joint 2d-3d self-supervised learning emerges spatial representations. In *NeurIPS*, 2025.
- [41] Zheyuan Zhou, Le Wang, Naiyu Fang, Zili Wang, Lemiao Qiu, and Shuyou Zhang. R3d-ad: Reconstruction via diffusion for 3d anomaly detection. In *European conference on computer vision*, pages 91–107. Springer, 2024.